Science of Sintering, **47** (2015) 259-268

doi: 10.2298/SOS1503259K

UDK 676.017.5; 669.018

The Thermal and Magnetic Properties of the $Fe_{89.8}Ni_{1.5}Si_{5.2}B_3C_{0.5}$ and $Fe_{81}B_{13}Si_{14}C_2$ Amorphous Alloys

A. Kalezić-Glišović[1*)], N. Mitrović[1], N. Obradović[2]

[1]Joint Laboratory for Advanced Materials of SASA, Section for Amorphous Systems, Faculty of Technical Sciences Čačak, University of Kragujevac, Svetog Save 65, 32 000 Čačak, Serbia

[2] Institute of Technical Sciences of SASA, Knez Mihailova 35, 11 000 Belgrade, Serbia

Abstract:

This paper investigates the thermal and magnetic properties of two iron based amorphous alloys with different Fe-content: $Fe_{89.8}Ni_{1.5}Si_{5.2}B_3C_{0.5}$ and $Fe_{81}B_{13}Si_{14}C_2$. The XRD results show that the thermal induced structural changes occur in the temperature range of 300^0C – 850^0C for the $Fe_{89.8}Ni_{1.5}Si_{5.2}B_3C_{0.5}$ amorphous alloy. The appearance of the first crystallization peaks on DSC thermograms of $Fe_{81}B_{13}Si_4C_2$, amorphous alloy is perceived already at 450^0C. The initial magnetization curves of the as-cast sample of the $Fe_{89.8}Ni_{1.5}Si_{5.2}B_3C_{0.5}$ amorphous alloy, obtained at the frequencies of 50 Hz, 400 Hz and 1000 Hz show the excellent match. The maximum relative magnetic permeability for $Fe_{89.8}Ni_{1.5}Si_{5.2}B_3C_{0.5}$ alloy sample is achieved at magnetic field strength of about 20 A/m for all frequencies, whereas the values of about 7000 were obtained at the frequencies of 50 Hz and 400 Hz. The influence of frequency on total power losses, for both alloys exhibits the increase of core losses with frequency increase. The amorphous alloy $Fe_{89.8}Ni_{1.5}Si_{5.2}B_3C_{0.5}$ toroidal core exhibits about 3 time higher total power losses.

Keywords: *Thermal properties, Magnetic properties, Initial magnetization curve, Hysteresis loops, Total power core losses.*

1. Introduction

Iron based amorphous and nanocrystalline alloys are well established commercial soft-magnetic materials as their properties ratio vs. prices is well acceptable in common electrical devices. There are still intensive research efforts of their sensors effects as a single used ribbon [1, 2] or as a combination of amorphous ribbon with piezofiber [3, 4] or magnetostrictive [5] laminates as a new generation of multifunctional materials. Metglas/PMN-PT fiber laminates as an excellent magnetoelectric composite for low noise sensor of ultralow magnetic field were presented at operating frequency f = 1 Hz [3].

Also, the investigations with two interesting goals are still actually due to reducing size of transformers: the increase of magnetic induction and decrease of coercive force [6, 7], i.e. the improvement of permeability and power losses. The first task was solved with the increasing atomic percentage of the iron content, i.e. with the substantial iron content over 80% that is the most probably position of the eutectic minimum in Fe-M (M-metalloid)

*) **Corresponding author**: aleksandra.kalezic@ftn.kg.ac.rs

systems.

Iron based nanocrystalline alloys exhibit excellent soft magnetic properties, low coercivity, high permeability and therefore low power losses [8]. For instance, there is very perspective commercial alloy $Fe_{81.2}Co_4Si_{0.5}B_{9.5}P_4Cu_{0.8}$ NANOMET with core losses of about 0.15 W/kg at 50 Hz and at 0.6 T [9]. Interesting soft magnetic properties of MnZn ferrites were obtained by optimization of powder injection molding technology [10]; however these ferrites have low values of saturation magnetic induction B_s.

In this paper is presented the comparison of magnetic properties of two iron based amorphous alloys with different Fe-content. The first alloy is the commercial composition $Fe_{81}B_{13}Si_{14}C_2$ and the second one is the alloy with significantly increased iron content $Fe_{89.8}Ni_{1.5}Si_{5.2}B_3C_{0.5}$.

2. Experimental

Ribbon shaped samples of the investigated amorphous alloys were obtained using the standard procedure of rapid quenching of the melt on a rotating disc (melt-spinning). The obtained ribbons were 2 cm wide and 35 μm thick. Thermal stability was investigated in a nitrogen atmosphere by the differential scanning calorimetry method (DSC) using SHIMADZU DSC-50 analyzer in the temperature region from room temperature to 600^0C. X-ray investigations were performed using Cu-K_α radiation lines (λ = 0.154178 nm) on a Phillips PW1710 device. B-H hysteresis loops were measured on toroidal core samples at different frequencies of sinusoidal excitation and at different magnetic fields for both alloys by Brockhaus MPG 100D measuring system.

3. Results and discussion

In our previous papers [11, 12] it was shown that the amorphous alloy $Fe_{89.8}Ni_{1.5}Si_{5.2}B_3C_{0.5}$ crystallizes within the temperature range from 520^0C to 620^0C. Therefore, the process of the structural relaxation was studied at temperatures for 100 – 150^0C lower than the initial crystallization temperature. XRD patterns of the $Fe_{89.8}Ni_{1.5}Si_{5.2}B_3C_{0.5}$ and $Fe_{81}B_{13}Si_{14}C_2$ samples are shown in the diagrams on Fig. 1.

Fig. 1a shows XRD difractograms of the as-cast samples and samples annealed at 300^0C and 540^0C for 60 minutes of the $Fe_{89.8}Ni_{1.5}Si_{5.2}B_3C_{0.5}$alloy. Annealing of alloy samples were performed in quartz ampoule which were further vacuumed and isothermally treated for 60 minutes. Based on the wide peak in the range of the diffraction angles 2θ of 40^0 – 50^0, it may be determined that the as-cast $Fe_{89.8}Ni_{1.5}Si_{5.2}B_3C_{0.5}$ (Fig. 1a) and $Fe_{81}B_{13}Si_{14}C_2$ (Fig.1b) alloy samples are characterized by high level of amorphousness. Due to presence of small percentage of matalloides (Si, B, C below 10%), as-cast samples are not fully amorphous, as amorphous matrix features residual crystallites upon obtaining. Amorphous structure remains unchanged during the alloy heating at 300 ^{0}C (Fig. 1a). For better understanding of the crystallization process, the analysis of the X-ray difractogram of $Fe_{89.8}Ni_{1.5}Si_{5.2}B_3C_{0.5}$ alloy samples was conducted, which had been isothermally heated in the temperature range from 300^0C to 850^0C, showing that the thermal induced structural changes occur in this temperature region. Fig. 1b shows the X-ray difractograms of the as-cast samples and samples annealed at 450^0C and 700^0C during 60 minutes of the alloy

$Fe_{81}B_{13}Si_{14}C_2$. Amorphous structure remains unchanged at annealing of this alloy at the temperature of 400^0C [13]. The appearance of the first crystallization peaks on difractograms of $Fe_{81}B_{13}Si_4C_2$ alloy samples is perceived at 450 ^{0}C [14].

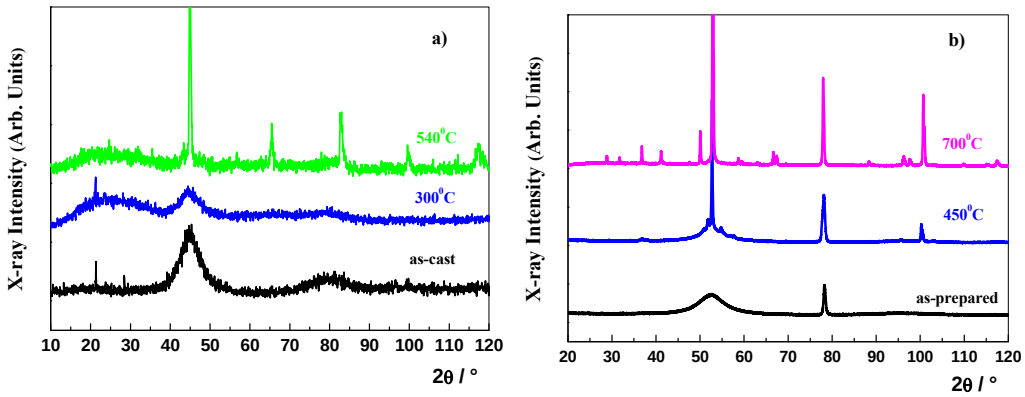

Fig. 1. XRD patterns of the a) $Fe_{89.8}Ni_{1.5}Si_{5.2}B_3C_{0.5}$ and b) $Fe_{81}B_{13}Si_{14}C_2$ samples.

The thermal stability of the $Fe_{89.8}Ni_{1.5}Si_{5.2}B_3C_{0.5}$ [12] and $Fe_{81}B_{13}Si_4C_2$ alloy samples was investigated by DSC in the temperature interval of 20^0C – 600^0C, at the heating rate of 20^0C/min. Fig. 2 shows DSC thermogram of the $Fe_{81}B_{13}Si_4C_2$ as-cast alloy sample.

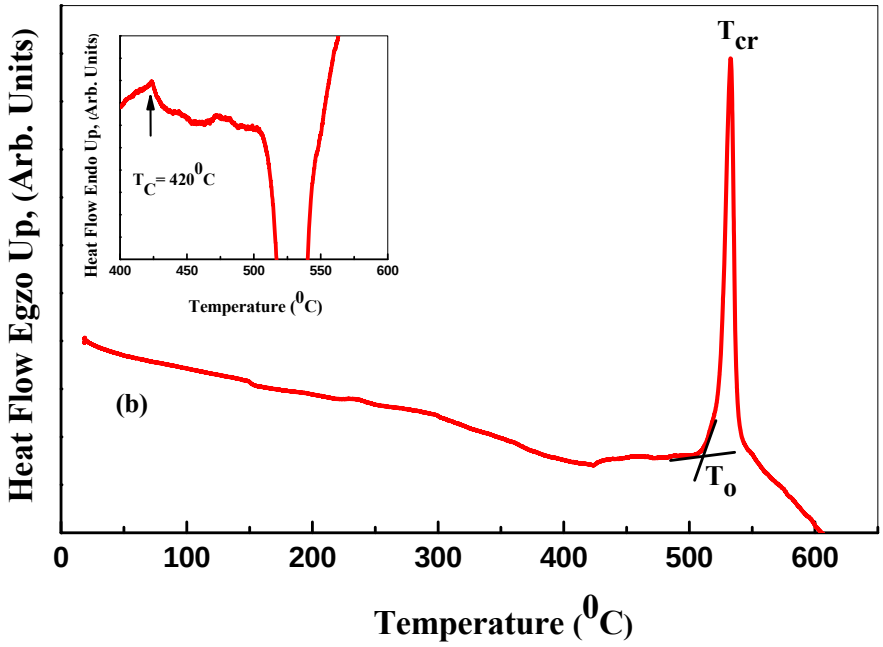

Fig. 2. DSC thermogram of the $Fe_{81}B_{13}Si_4C_2$ amorphous alloy obtained at heating rate of 20 ^{0}C/min (arrow denote endo -peak i.e. Curie temperature).

Fig. 3 shows magnetization curves of the as-cast sample of the $Fe_{89.8}Ni_{1.5}Si_{5.2}B_3C_{0.5}$ amorphous alloy, obtained at the frequencies of 50 Hz, 400 Hz and 1000 Hz. As it can be noticed, all three curves exhibit the excellent match.

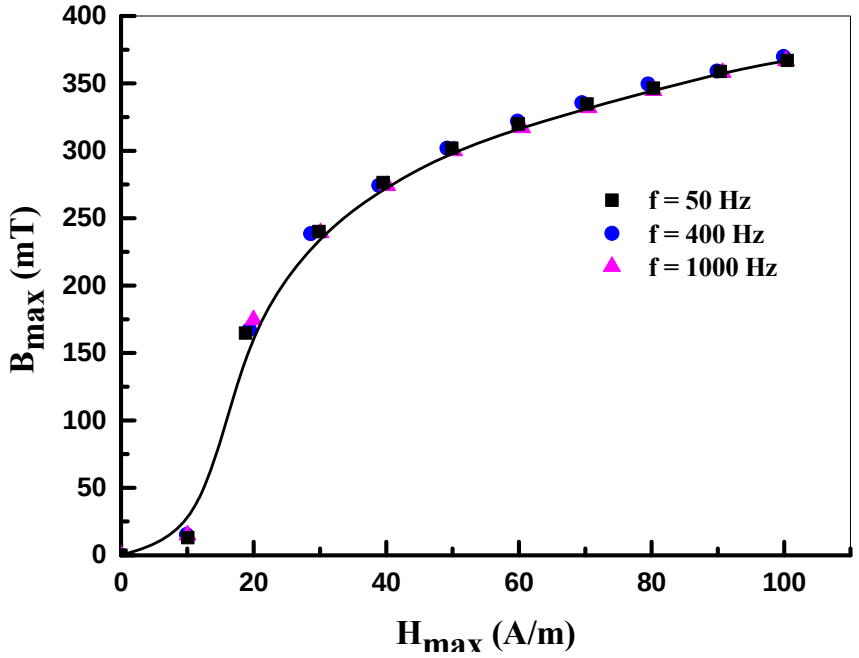

Fig. 3. The initial magnetization curves of as-cast sample of $Fe_{89.8}Ni_{1.5}Si_{5.2}B_3C_{0.5}$ amorphous alloy at frequencies of 50 Hz, 400 Hz and 1000 Hz.

Fig. 4 shows dependence of the relative magnetic permeability ($\mu_r = \mu/\mu_0$) over the external magnetic field strength at the frequencies of 50 Hz, 400 Hz and 1000 Hz for $Fe_{89.8}Ni_{1.5}Si_{5.2}B_3C_{0.5}$ as-cast amorphous alloy sample. Maximum relative magnetic permeability is achieved at magnetic field strength of about 20 A/m for all three frequencies, whereas the highest values of about 7000 are obtained at frequencies of 50 Hz and 400 Hz.

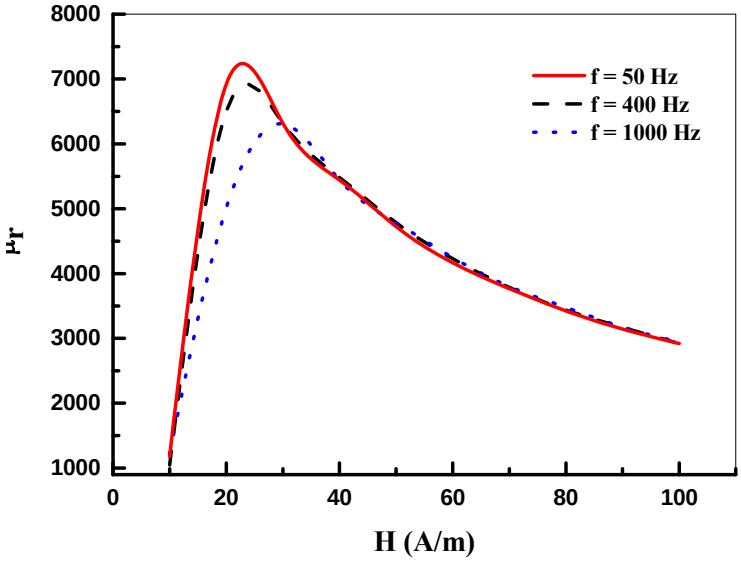

Fig. 4. The relative magnetic permeability dependence on external magnetic field at frequencies of 50 Hz, 400 Hz and 1000 Hz.

Fig. 5 shows hysteresis loops B-H of $Fe_{89.8}Ni_{1.5}Si_{5.2}B_3C_{0.5}$ as-cast alloy sample, obtained at H_{max} = 100 A/m and sinusoidal excitation of the frequencies of 5, 50, 100, 400, 800 and 1000 Hz. These hysteresis loops have R form with remanence ratio $B_r/B_s \approx 0.75$.

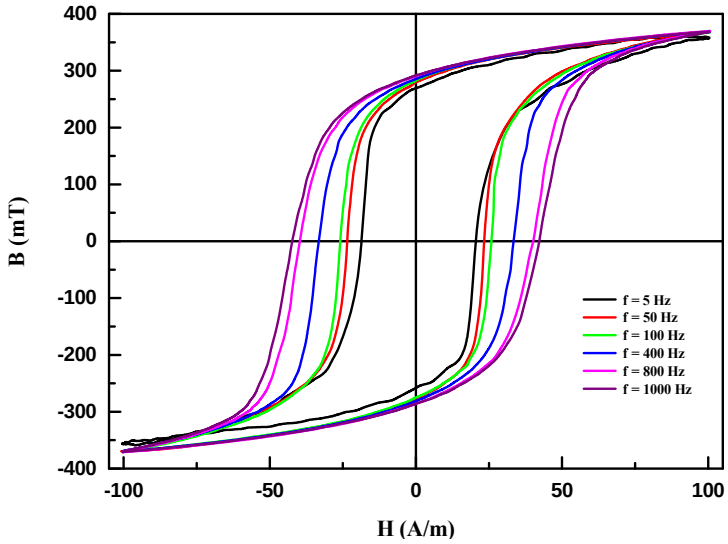

Fig. 5. The hysteresis loops of the $Fe_{89.8}Ni_{1.5}Si_{5.2}B_3C_{0.5}$ toroidal sample in as-cast state at different frequencies (from 5 Hz to 1000 Hz) and H_{max} = 100 A/m.

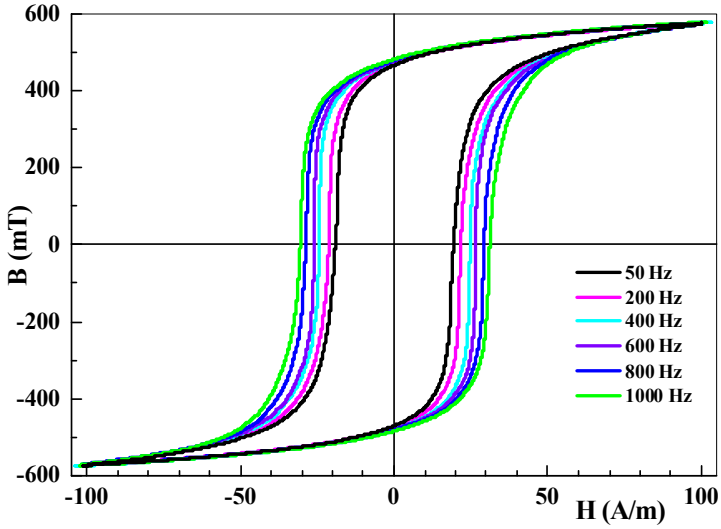

Fig. 6. The hysteresis loops of the $Fe_{81}B_{13}Si_4C_2$ toroidal sample in as-cast state at different frequencies (from 50 Hz to 1000 Hz) and H_{max} = 100 A/m.

Hysteresis B-H loops has been monitored for the as-cast $Fe_{81}B_{13}Si_4C_2$ torus-shaped alloy samples as well. The frequency effect on hysteresis loops at H_{max} = 100 A/m and the sinusoidal excitation of 50, 200, 400, 600, 800 and 1000 Hz is shown on Fig. 6 [14].

As it can be observed from the Fig. 5 and Fig. 6, the hysteresis loops become wider and magnetic losses increase with frequency increase. Such dependence is caused by eddy currents and at higher frequencies by spin relaxation processes. It can be noticed on Fig. 6 that hysteresis loops of the $Fe_{81}B_{13}Si_4C_2$ alloy have higher remanence ratio ($B_r/B_s \approx 0.8$), that is a

significant advantage of this magnetic material for the application in electrical devices. Further, the significant increase of iron content in amorphous alloy $Fe_{89.8}Ni_{1.5}Si_{5.2}B_3C_{0.5}$ is followed with the increase of coercivity.

Fig. 7 shows hysteresis loops of the $Fe_{89.8}Ni_{1.5}Si_{5.2}B_3C_{0.5}$ as-cast alloy sample, obtained at the same frequency of 50 Hz, but at different magnetic field strengths of 1000 A/m, 2000 A/m and 3000 A/m. It can be noticed almost the same value of the remanence $B_r \approx 0.33$ T.

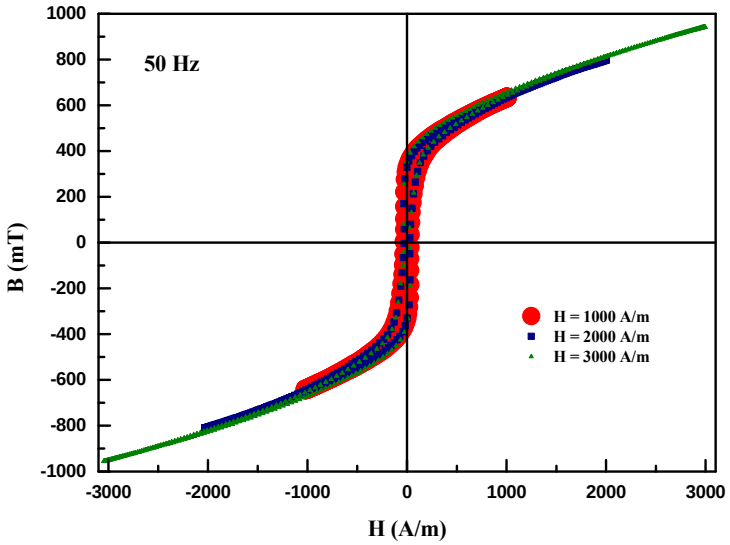

Fig. 7. The hysteresis loops of the $Fe_{89.8}Ni_{1.5}Si_{5.2}B_3C_{0.5}$ toroidal sample in as-cast state at frequency of 50 Hz and at different magnetic fields (from 1000 A/m to 3000 A/m).

Fig. 8 shows hysteresis loops of the $Fe_{89.8}Ni_{1.5}Si_{5.2}B_3C_{0.5}$ as-cast alloy sample, obtained at different frequencies of 50 Hz, 400 Hz and 1000 Hz and at different magnetic field strengths from 10 A/m to 100 A/m.

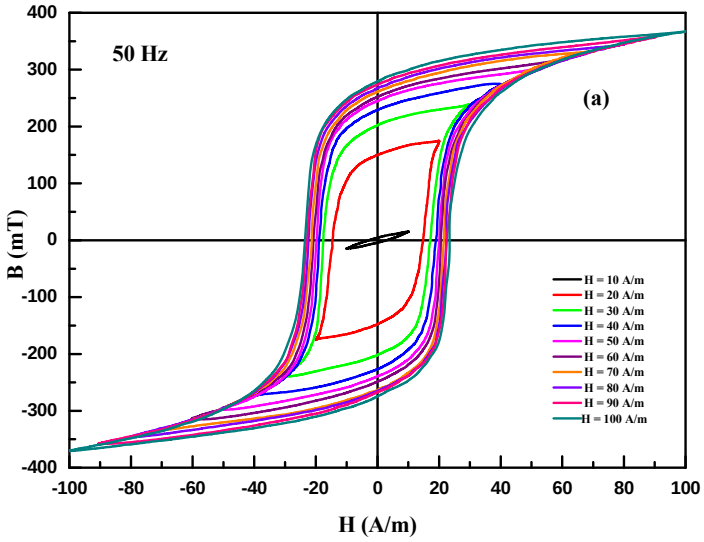

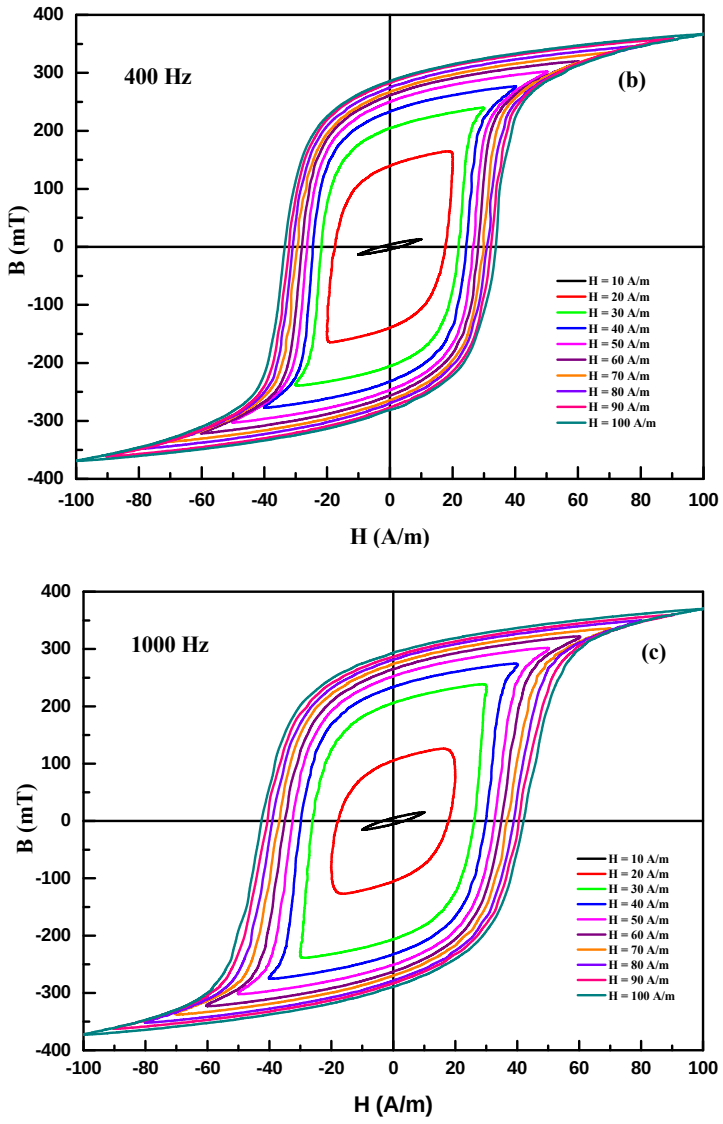

Fig. 8. The hysteresis loops of the $Fe_{89.8}Ni_{1.5}Si_{5.2}B_3C_{0.5}$ toroidal sample in as-cast state at frequencies of a) 50 Hz, b) 400 Hz and c) 1000 Hz and at different magnetic fields.

It can be noticed on Fig. 8 that the hysteresis loops of the as-cast $Fe_{89.8}Ni_{1.5}Si_{5.2}B_3C_{0.5}$ alloy sample get wider with the increase in frequency, while the increase in the surface area of these loops results in the increased power core losses.

The total core losses are proportional to the surface area of hysteresis loop and consist of two components: hysteresis losses P_h and eddy current losses P_e, i.e. $P_s = P_h + P_e$.

Hysteresis losses are proportional to the frequency (~ f):

$$P_h = \eta \cdot f \cdot m \cdot B_m^2, \quad (1)$$

where: η - Steinmetz hysteresis coefficient,

f - frequency,

B_m - maximum magnetic flux density,

m – toroidal corre mass.

Eddy-current losses are proportionally to the square of frequency (~ f^2):

$$P_w = \sigma \cdot f^2 \, m \cdot B_m^2, \quad (2)$$

where σ is parameter that involve thickness, resistivity and density of material.

The comparison of the frequency dependence of total power losses P_s referred to the core mass for both investigated alloys is shown on Fig. 9.

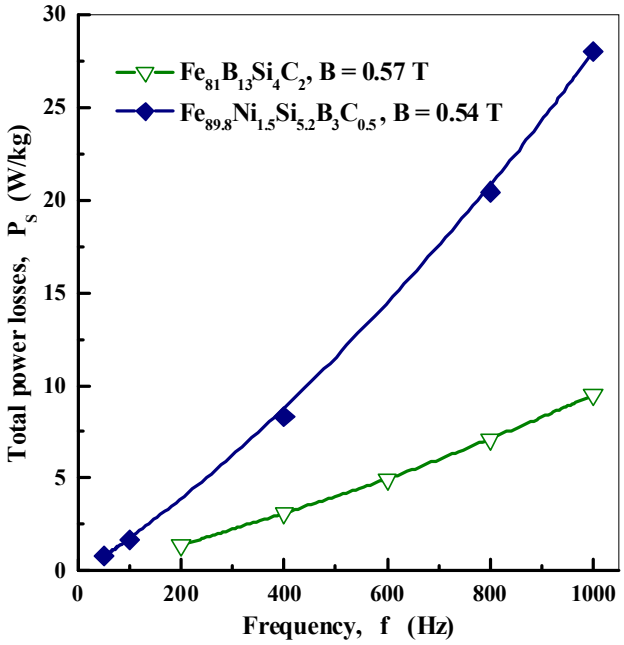

Fig. 9. Total power losses P_s referred to the core mass for the $Fe_{89.8}Ni_{1.5}Si_{5.2}B_3C_{0.5}$ and the $Fe_{81}B_{13}Si_4C_2$ amorphous alloys.

As it can be noticed the $Fe_{81}B_{13}Si_4C_2$ amorphous alloy toroidal core exhibits about 3 times lower total power losses. The significant increase of iron content in the amorphous alloy $Fe_{89.8}Ni_{1.5}Si_{5.2}B_3C_{0.5}$ is followed with the increase of coercivity as a result of more intensive magnetic domain pinning effect and therefore with the increase of total core power losses.

Total core losses of the amorphous alloy $Fe_{89.8}Ni_{1.5}Si_{5.2}B_3C_{0.5}$ are 0.8 W/kg at 50 Hz and at 0.54 T that is 2 times higher in comparison with commercially non-oriented magnetic steel [9].

4. Conclusion

The comparison of magnetic properties of two iron based soft magnetic amorphous ribbons with different Fe-content was perfomed. The first alloy is the commercial composition $Fe_{81}B_{13}Si_{14}C_2$ and the second one is the alloy with significantly increased iron content $Fe_{89.8}Ni_{1.5}Si_{5.2}B_3C_{0.5}$. The initial magnetization curves of the as-cast sample of the $Fe_{89.8}Ni_{1.5}Si_{5.2}B_3C_{0.5}$ amorphous alloy, obtained at the frequencies of 50 Hz, 400 Hz and 1000 Hz show the excellent match. The maximum relative magnetic permeability for $Fe_{89.8}Ni_{1.5}Si_{5.2}B_3C_{0.5}$ alloy sample is achieved at magnetic field strength of about 20 A/m and the values of about 7000 are obtained at the frequencies of 50 Hz and 400 Hz. The hysteresis loops of both alloys become wider and therefore the core losses increase with frequency increase due to eddy currents and spin relaxation at higher frequencies. It can be noticed that hysteresis loops of the $Fe_{81}B_{13}Si_4C_2$ alloy have higher remanence ratio ($B_r/B_s \approx 0.8$) than the $Fe_{89.8}Ni_{1.5}Si_{5.2}B_3C_{0.5}$ alloy ($B_r/B_s \approx 0.75$), that is a significant advantage of this magnetic material for the application in electrical devices. The significant increase of iron content in the

amorphous alloy $Fe_{89.8}Ni_{1.5}Si_{5.2}B_3C_{0.5}$ is followed with the increase of coercivity as a result of more intensive magnetic domain pinning effect and therefore with the increase of total core power losses.

Acknowledgements

The financial support from the Ministry of Education, Science and Technological Development of the Republic of Serbia through Project No. 172057 is acknowledged.

References

1. N. Mitrović, S. Kane, S. Roth, A. Kalezić-Glišović, C. Mickel, and J. Eckert, "The Precipitation of Nanocrystalline Structure in Joule Heated $Fe_{72}Al_5Ga_2P_{11}C_6B_4$ Metallic Glasses", Journal of Minning and Metallurgy, Section B: Metallurgy, Vol. 48 (2012), pp. 319.
2. V. Chunchua, and G. Markandeyulu, "Magnetoimpedance studies in as-quenched $Fe_{73.5}Si_{13.5}B_8CuV_{3-x}AlNb_x$ nanocrystalline ribbons", Journal of Applied Physics, Vol. 113(17) (2013) A321.
3. Y. Wang, J. Li, and D. Viehland, „Magnetoelectrics for Magnetic Sensor Applications: Status, Challenges and Perspectives", Materials Today, Vol. 17(6) (2014), pp. 269.
4. J. Qiu, Y. Wen, P. Li, and H. Chen, „The Giant Magnetoelectric Effect in $Fe_{73.5}Cu_1Nb_3Si_{13.5}B_9$ /PZT Thick Film Composites", Journal of Applied Physics, Vol. 117 (2015), pp. 17D701.
5. Y. Jia, C. Zheng, Z. Wu, R. K. Zheng, Y. Fang, Y. Zhang, and H. Li, "Enhanced magneto-impedance in $Fe_{73.5}Cu_1Nb_3Si_{13.5}B_9$ ribbons from laminating with magnetostrictive terfenol-D alloy plate", Applied Physics Letters, Vol. 101 (17) (2012), pp. 251914.
6. R. Hasegawa and D. Azuma, "Impacts of amorphous metal-based transformers on energy efficiency and environment", Journal of Magnetism and Magnetic Materials, Vol. 320(20) (2008), pp. 2451.
7. D. Azuma, R. Hasegawa, S. Saito and M. Takahashi, "Effect of residual strain in Fe-based amorphous alloys on field induced magnetic anisotropy and domain structure", Journal of Applied Physics, Vol. 113 (2013), pp. 17A339.
8. M. Willard, M. Daniil, "Nanocrystalline Soft Magnetic Alloys Two Decades of Progress", Handbook of Magnetic Materials, Vol. 21 (2013), pp. 173–342.
9. K. Takenaka, A. D. Setyawan, Y. Zhang, P. Sharma, N. Nishiyama and A. Makino, „Production of Nanocrystalline (Fe,Co)-Si-B-P-Cu Alloy with Excellent Soft Magnetic Properties for Commercial Applications", Materials Transactions, Vol. 56(3) (2015), pp. 372.
10. B. Zlatkov, N. Mitrović, M. V. Nikolić, A. Maričić, H. Danninger, O. Aleksić, E. Halwax, "Properties of MnZn ferrites prepared by powder injection molding technology", Materials Science and Engineering B, Vol. 175 (3) (2010), pp. 217.
11. A. Kalezić-Glišović, L. Novaković, A. Maričić, D. Minić, N. Mitrović, "Investigation of Structural Relaxation, Crystallization Process and Magnetic Properties of Fe-Ni-Si-B-C Amorphous Alloy", Materials Science and Engineering B, Vol. 131 (2006), pp. 45.
12. A.Kalezić-Glišović, Master thesis, Faculty of Physics, Belgrade, 2006.
13. A.Kalezić-Glišović, PhD thesis, Faculty of Physics, Belgrade, 2012.

14. S. Djukić, V. Maričić, A. Kalezić-Glišović, L. Ribić-Zelenović, S. Randjić, N. Mitrović, N. Obradović, "The Effect of Temperature and Frequency on Magnetic Properties of the $Fe_{81}B_{13}Si_4C_2$ Amorphous Alloy", Science of Sintering 43(2) (2011), pp. 175.

Садржај: *У овом раду испитивана су топлотна и магнетна својства двају аморфних легура са различитим процентом Fe: $Fe_{89.8}Ni_{1.5}Si_{5.2}B_3C_{0.5}$ и $Fe_{81}B_{13}Si_{14}C_2$. Резултати рендгеноструктурне анализе узорака легуре $Fe_{89.8}Ni_{1.5}Si_{5.2}B_3C_{0.5}$ показују да се термички изазване структурне појаве одвијају у температурској области од 300^0C – 850^0C. Појава првих кристализационих пикова на ДСЦ термограмима узорака легуре $Fe_{81}B_{13}Si_{14}C_2$ се запажа већ на 450 ^0C. Криве магнећења неодгреваног узорка легуре $Fe_{89.8}Ni_{1.5}Si_{5.2}B_3C_{0.5}$ добијене на фреквенцијама 50 Hz, 400 Hz и 1000 Hz показују одлично слагање. Максимална релативна магнетна пермеабилност узорка легуре $Fe_{89.8}Ni_{1.5}Si_{5.2}B_3C_{0.5}$ је добијена при јачини магнетног поља од 20 A/m за све три фреквенције, док је на фреквенцијама 50 Hz и 400 Hz добијена вредност пермеабилности од око 7000. Утицај фреквенције на магнетне губитке показује пораст губитака са повећањем фреквенције код обе легуре. Аморфна легура $Fe_{89.8}Ni_{1.5}Si_{5.2}B_3C_{0.5}$ има 3 пута већу вредност магнетних губитака од легуре $Fe_{81}B_{13}Si_{14}C_2$.*

Кључне речи: *термичка својства, магнетна својства, крива магнећења, хистерезисне петље, укупни губици снаге*